

Outlier detection by ensembling uncertainty with negative objectness

Anja Delić
anja.delic@fer.hr

Matej Grčić
matej.grcic@fer.hr

Šiniša Šegvić
snisa.segvic@fer.hr

University of Zagreb,
Faculty of Electrical Engineering and
Computing,
Zagreb, Croatia

Abstract

Outlier detection is an essential capability of safety-critical visual recognition. Many existing methods deliver good results by encouraging standard closed-set models to produce low-confidence predictions in negative training data. However, that approach conflates prediction uncertainty with recognition of outliers. We disentangle the two factors by revisiting the K+1-way classifier that involves K known classes and one negative class. This setup allows us to formulate a novel outlier score as an ensemble of in-distribution uncertainty and the posterior of the negative class that we term negative objectness. Our UNO score can detect outliers due to either high prediction uncertainty or similarity with negative training data. We showcase the utility of our method in experimental setups with K+1-way image classification and K+2-way dense prediction. In both cases we show that the bias of real negative data can be relaxed by leveraging a jointly trained normalizing flow. Our models outperform the current state-of-the-art on standard benchmarks for image-wide and pixel-level outlier detection.

1 Introduction

Modern machine learning [24, 36] delivers unprecedented performance on a plethora of academic datasets [16, 17, 63]. These evaluation protocols are often limited to instances of predetermined taxonomies [16, 75]. However, many objects in the real world do not belong to the training taxonomy. In such situations, standard algorithms for image recognition [68] and scene understanding [12, 14] may behave unpredictably [99].

Discriminative models may become robust to outliers through upgrade to open-set recognition [60]. This can be conveniently achieved by complementing standard classification with outlier detection [100]. Typically, the outlier detector delivers a scalar outlier score that induces ranking and enables detection through thresholding [80]. Many outlier detectors both in the image-wide [20, 39] and the pixel-level context [4, 5, 10, 30, 39] rely on negative training data. Although it cannot represent the entire variety of the visual world, the negative data can still help by signaling that not all data should be confidently recognized. If the variety of the negative data greatly exceeds the variety of the inliers, then there is a reasonable

hope that the test outliers will be detected. Unfortunately, this entails undesired bias towards test outliers that appear similar to the negative training data. This concern can be addressed either by relying on synthetic negatives [24, 57, 74], or through separate ranking with respect to approaches that do not train on real negative data [9, 9, 102].

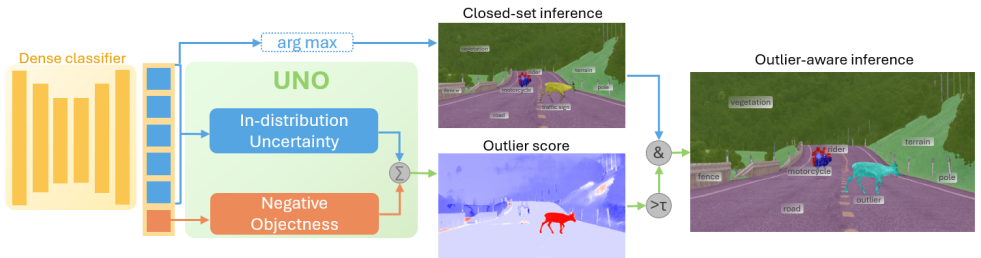


Figure 1: We propose UNO, a plug-in module that enables outlier-aware inference atop a desired feature extractor. UNO decouples in-distribution uncertainty from outlier recognition, and boosts the outlier detection performance by ensembling the two components.

Many existing methods improve open-set performance of existing closed-set models by encouraging low-confidence predictions in negative training data [42, 57]. However, this approach conflates prediction uncertainty with outlier recognition. In this paper, we disentangle the two factors by reconsidering the $K+1$ -way classifier where the additional class represents the negative data. This allows us to formulate the outlier score as the posterior of the $K+1$ -th class, which we term negative objectness. Moreover, the outlier score can also be formulated as prediction uncertainty over the K known classes [42]. We find that these two formulations exhibit complementary behaviour due to being sensitive to different test outliers. Consequently, we propose a novel outlier score that we term UNO: ensemble of *Uncertainty over K inlier classes* [58] and *Negative Objectness*.

Our UNO score is a strikingly good fit in the pixel-level context as an extension of some direct set-prediction approach [8]. We express the negative objectness as the posterior of the negative class in the frame of a $K+2$ -way mask-level classifier [14, 59, 96]. A closer look suggests that our score performs well due to different inductive bias of the two components as indicated by a remarkably weak correlation. The UNO score performs competitively in the image-wide context as well, even though the absence of the no-object class decreases the synergy of the two components. Our models outperform the state-of-the-art on several standard benchmarks in both learning setups, *i.e.* with and without real negative data.

2 Related work

Image-wide setup. Image-wide classification models can be complemented with outlier detection either through a modified training procedure or in a post-hoc manner with frozen parameters [102]. Post-hoc methods build upon pre-trained closed-set classifiers. Early baselines express the outlier score as maximum softmax probability [57] or maximum logit [40]. TempScale [58] calibrates softmax probabilities with temperature scaling while ODIN [61] pre-processes the input with anti-adversarial perturbations. Recent post-hoc methods simplify layer activations [23] or fit generative models to pre-logit features [87, 96, 103]. In contrast, training methods involve various regularizations that either consider only inlier

data or utilize real negative data as well. The former rely on modeling confidence [49], self-supervised training [41, 86], per-sample temperature scaling [45], outlier synthesis in feature space [25, 53, 88] or mitigating overconfidence [94]. Recent methods guide the learning process with respect to nearest neighbours [77] or leverage distances in feature space either by combining different distance functions [76] or distances in different feature spaces [13]. Early work in training with negative data [20, 69] encourages high entropy in inlier samples. MCD [97] promotes discrepancy between prediction on OOD samples of two classification heads. UDG [95] groups negative data following inlier taxonomy to enrich semantic knowledge of inlier classes. MixOE [101] interpolates between inliers and negatives to improve regularization. Unlike related training-based methods, UNO does not modify the standard classifier training objective, but merely requires a slight architectural change to extend the classifier with a logit for the negative class. Moreover, empirical insights suggest that UNO requires significantly less negative data than related methods.

Dense prediction. Many image-wide outlier detection methods can directly complement models for pixel-level prediction [57, 40]. Early approaches estimate the prediction uncertainty with maximum softmax probability [58], ensembling [55] or Bayesian uncertainty [72]. Subsequent work suggests energy scores [55] and the standardized max-logit score [48]. Training with negative data can be incorporated by pasting negative content from broad negative datasets (ImageNet [8], ADE20K [107] or COCO [52]) atop inlier images [4, 6, 10, 30, 69, 89]. However, real negative data can be replaced with synthetic negative patches obtained by sampling a jointly trained generative model [57, 74, 105]. Outlier detection performance can be further improved by providing more capacity [91]. Another branch of methods considers generative models [4, 30, 50].

Mask-level recognition. Recent panoptic architectures [14, 59, 96] decompose scene understanding into class-agnostic segmentation and region-wide recognition. They frame the detection of semantic masks as direct set-prediction where each mask is classified into K inlier classes and one no-object class. This induces a degree of openness and therefore favours outlier detection. Recent work shows great applicability of the Mask2Former architecture for open-set segmentation [10, 51, 73, 78]. All these methods detect anomalies due to not belonging to any inlier class and improve when training with negative data. Specifically, RbA [73] reduces energy in negative pixels, Mask2Anomaly [78] uses a contrastive loss, while EAM [51] ensembles region-wide outlier scores. However, these approaches conflate negative data with no-object regions. Furthermore, they fail to exploit the fact that mask queries behave like one-vs-all classifiers [10, 73], which makes them appropriate for direct detection of anomalous regions. UNO addresses these weaknesses by decoupling negatives from the no-object class, and representing them as a standalone class in the $K+2$ -way taxonomy.

3 Disentangling negative objectness from uncertainty

Let $h_{\theta_1} : \mathcal{X} \rightarrow \mathbb{R}^d$ be a feature extractor (e.g. ResNet [56] or ViT [24]) onto which we attach our $K+1$ -way classifier $g_{\theta_2} : \mathbb{R}^d \rightarrow \Delta^K$, where \mathcal{X} is the input space and Δ^K is a K -dimensional probabilistic simplex. Given an input $\mathbf{x} \in \mathcal{X}$, we compute a latent representation $\mathbf{z} = h_{\theta_1}(\mathbf{x})$ and map it onto the simplex point $\mathbf{p} = \text{softmax}(g_{\theta_2}(\mathbf{z}))$. Thus, our deep model $f_{\theta} = g_{\theta_2} \circ h_{\theta_1}$ maps input samples from \mathcal{X} onto simplex points in Δ^K . We assume that the classifier g_{θ_2} is

a simple projection. Thus we have $g_{\theta_2}(\mathbf{x}) = \mathbf{W} \cdot \mathbf{x}$, where the rows of \mathbf{W} correspond to class vectors \mathbf{w}_j .

Negative objectness. Given feature representation \mathbf{z} and a linear classifier g , we formulate the negative objectness score (\mathbf{s}_{NO}) as posterior of the $K+1$ -th class:

$$\mathbf{s}_{\text{NO}}(\mathbf{z}) := P(Y = K+1|\mathbf{z}) = \frac{\exp(\mathbf{w}_{K+1}^T \mathbf{z})}{\sum_{j=1}^{K+1} \exp(\mathbf{w}_j^T \mathbf{z})}. \quad (1)$$

The \mathbf{s}_{NO} score tests whether a given sample is semantically dissimilar from the inlier classes and similar to the negative training data. Consequently, a test outlier that is similar to the training negatives will yield high \mathbf{s}_{NO} .

Prediction uncertainty. Negative objectness is not suitable for detecting test outliers that are semantically dissimilar from the negative training data. However, many of these outliers yield uncertain predictions across inlier classes of our $K+1$ -classifier. We address this observation by defining the uncertainty score as negative prediction confidence across the K inlier classes:

$$\mathbf{s}_{\text{Unc}}(\mathbf{z}) := - \max_{k=1\dots K} P(Y = k|\mathbf{z}) = - \max_{k=1\dots K} \frac{\exp(\mathbf{w}_k \mathbf{z})}{\sum_{j=1}^{K+1} \exp(\mathbf{w}_j \mathbf{z})} = - \frac{\exp(\mathbf{w}_{\hat{k}} \mathbf{z})}{\sum_{j=1}^{K+1} \exp(\mathbf{w}_j \mathbf{z})}. \quad (2)$$

The last equality in (2) denotes the index of the winning class as $\hat{k} = \operatorname{argmax}_k \exp(\mathbf{w}_k^T \mathbf{z})$. The uncertainty score \mathbf{s}_{Unc} detects different outliers than negative objectness \mathbf{s}_{NO} despite attending to the same shared features \mathbf{z} .

UNO score. We integrate the prediction uncertainty (2) and negative objectness (1) into the UNO score as the sum of the two terms:

$$\mathbf{s}_{\text{UNO}}(\mathbf{z}) = \mathbf{s}_{\text{Unc}}(\mathbf{z}) + \mathbf{s}_{\text{NO}}(\mathbf{z}). \quad (3)$$

UNO has an interesting geometrical interpretation in the pre-logit space \mathbb{R}^d . Class vectors tend to be mutually orthogonal: $\mathbf{w}_i^T \mathbf{w}_j = 0$, $\forall i, j \in \{1, 2, \dots, K+1\}$ [23]. This arrangement is enforced by the standard supervised loss ($-\log \text{softmax}$) whenever there is enough data, and enough capacity and dimensionality ($d > K+1$) in the feature extractor h_{θ_1} . Thus, a small angle between the latent representation \mathbf{z} and the negative vector \mathbf{w}_{K+1} leads to high outlier objectness \mathbf{s}_{NO} . On the other hand, the uncertainty score \mathbf{s}_{Unc} is negatively correlated with the feature norm $\|\mathbf{z}\|$. If we fix the direction of \mathbf{z} , its norm can be viewed as reciprocal softmax temperature. As usual, large temperatures lead to uncertain predictions [24].

The above insights show that the two components of our score will be at least partially decorrelated due to being sensitive to different outliers: \mathbf{s}_{NO} detects large feature norms and good alignment with \mathbf{w}_{K+1} , while \mathbf{s}_{Unc} detects small feature norms and poor alignment with inlier vectors. Thus, the UNO score is likely to achieve lower error than any of the two components alone. Figure 2 illustrates our insight in an image-wide recognition experiment on small images. Further empirical analysis indicates a weak positive correlation between the UNO components, as detailed in the Appendix.

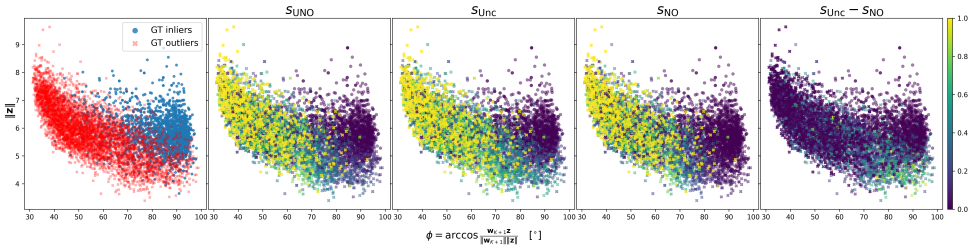


Figure 2: Interpretation of UNO in the pre-logit space \mathbb{R}^d in an OpenOOD ([10]) experiment with CIFAR-10 inliers. Small L_2 norm of feature representations \mathbf{z} leads to high s_{UNc} while the angle between \mathbf{z} and the $K+1$ -th weight vector \mathbf{w}_{K+1} leads to high s_{NO} . The two components capture different outliers as shown on the rightmost plot.

Extending UNO for dense prediction. The UNO outlier detector can be attached to any pre-trained deep classifier. In the case of image-wide prediction, we simply extend a pre-trained K -way classifier with an additional class. However, in the case of dense prediction, many contemporary architectures rely on mask-level recognition ([4]). Consequently, we build our per-pixel score by averaging the mask-level UNO scores:

$$\mathbf{s}_{\text{UNO}}^{\text{M2F}} = \sum_{i=1}^N \mathbf{m}_i \cdot \mathbf{s}_{\text{UNO}}(\mathbf{z}_i). \quad (4)$$

Note that equation 4 assumes that the dense prediction model has partitioned the input image into N different masks \mathbf{m}_i with the corresponding latent mask embeddings \mathbf{z}_i .

We note that the mask-level classifiers already use the $K+1$ -th logit to indicate that the particular query has not been associated with any image region. It would be a bad idea to reuse that logit for mask-level negative objectness since unused queries are regular occurrences in in-distribution images. Consequently, we extend the default classifier with the negative class. In our implementations, the $K+1$ -th logit corresponds to negative objectness while the $K+2$ -th logit indicates the no-object class. Please find more details in the Appendix.

4 Training UNO with and without real negative data

Let $\mathcal{D}_{\text{in}} = \{(\mathbf{x}_i, y_i)\}_{i=1}^{N^+}$ be an inlier dataset with $\mathbf{x} \in \mathcal{X}$ and $y_i \in \mathcal{Y}$, where \mathcal{Y} is the set of classes of size $K = |\mathcal{Y}|$. Let $\mathcal{D}_{\text{out}} = \{\mathbf{x}_j\}_{j=1}^{N^-}$ be a negative dataset that mimics test outliers. We construct a mixed-content training set \mathcal{D} as the union of inlier samples with negative samples labeled as the $K+1$ -th class: $\mathcal{D} = \mathcal{D}_{\text{in}} \cup \{(\mathbf{x}_j, K+1) \mid \mathbf{x}_j \in \mathcal{D}_{\text{out}}\}$.

We start from a K -way classifier that is pre-trained on inlier data \mathcal{D}_{in} as a part of an off-the-shelf model. We append the $K+1$ -th class and fine-tune the classifier f_θ on the mixed-content dataset \mathcal{D} by optimizing the standard cross-entropy loss:

$$L_{\text{cls}}(\theta) = \mathbb{E}_{\mathbf{x}, y \in \mathcal{D}} [-\ln P(y|\mathbf{x})]. \quad (5)$$

Every training minibatch contains an equal number of samples for all $K+1$ classes. Thus, we expose our model to significantly less negative data than the alternative approaches ([58], [9], [7], [10]), which utilize $2\times$ more negatives than inliers. Even though the outlier exposure of

our model is weak, it will still be biased towards detection of the test outliers that are similar to the training negatives. This issue can be circumvented by replacing the auxiliary negative dataset with synthetic negatives produced by a generative model [28, 57].

Synthetic negatives. We generate model-specific synthetic negatives by a normalizing flow f_ψ [27, 49] that we train alongside our discriminative classifier f_θ . We train the flow to generate samples that resemble inliers, but at the same time give raise to uncertain predictions across the inlier classes according to the following loss [32, 57]:

$$L_{\text{flow}}(\psi, \theta) = L_{\text{mle}}(\psi) + \beta \cdot L_{\text{jSD}}(\psi, \theta). \quad (6)$$

The first loss term $L_{\text{mle}}(\psi) = \mathbf{E}_{\mathbf{x}+\epsilon \in \mathcal{D}_{\text{in}}}[-\ln p_\psi(\mathbf{x})]$ maximizes the likelihood of inlier samples, while the second loss term $L_{\text{jSD}}(\psi, \theta) = \text{JSD}(U, f_\theta(\mathbf{x}))$ minimizes the Jensen-Shannon divergence between the uniform distribution and the predictions over the K inlier classes. The two competing objectives settle down when the generative model produces samples at the border of the inlier manifold [57]. The above loss jointly optimizes f_θ and f_ψ so that the discriminative model get aware of the negative class and thus preclude feature collapse [69]. Of course, the training also has to ensure that f_θ satisfies the primary discriminative loss.

However, a naive application of this recipe in the $K+1$ -way context would not work as intended. In fact, the generative loss (6) and the discriminative loss (5) would simply be satisfied by confident classification of all generated samples into the negative class. This trivial solution would embed the generated samples into a compact region of the feature space, and make them useless as proxies for outlier detection. Thus, we propose a two-step optimization procedure. The first step jointly trains f_ψ , f_θ , and the K inlier logits according to (6). The second step freezes the flow and fine-tunes the loss (5) in order to ensure recognition of generated negatives as the $K+1$ -th class. Different from previous approaches [32, 57], the loss (6) serves only to promote generation of useful synthetic negatives, while we ensure the outlier recognition quality by subsequent fine-tuning according to the loss (5).

Figure 3.a illustrates the learned latent representations as obtained by the two-step training procedure. Our synthetic negatives are sprinkled around the inlier manifold. Joint optimisation of the loss (6) and the $K+1$ -way cross-entropy loss (5) collapses synthetic negatives to a single mode, as shown in Figure 3.b. For reference, we also show the latent representations of the model trained with real negatives in Figure 3.c.

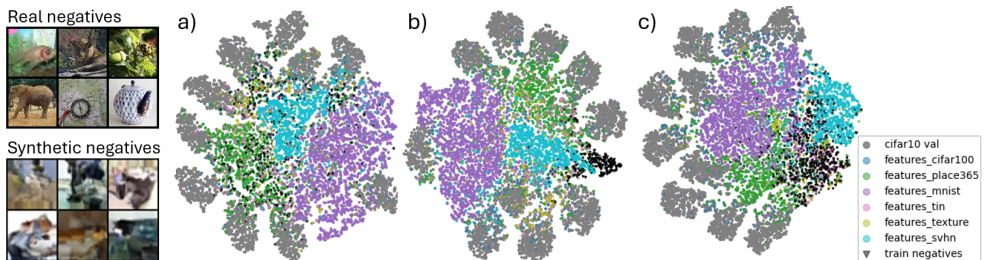


Figure 3: Left: Visualization of real and synthetic negatives from an OpenOOD CIFAR-10 experiment [102]. Right: t-SNE plots of the corresponding feature representations. Our two-set training strategy yields synthetic negatives near the inlier manifold (a), while the naive approach collapses synthetic negatives to a single mode (b). Relative location of real negatives indicate that they cover similar modes of test outliers as our synthetic samples (c).

Figure 4 shows our training approach in the dense prediction context. We paste negative training content atop the regular image to produce a mixed-content image. The mixed-content image is fed to the K+2-way classifier that optimizes the cross-entropy objective, similar as in the image-wide context. In the case of synthetic negatives, we jointly optimize the dense classifier and the normalizing flow.

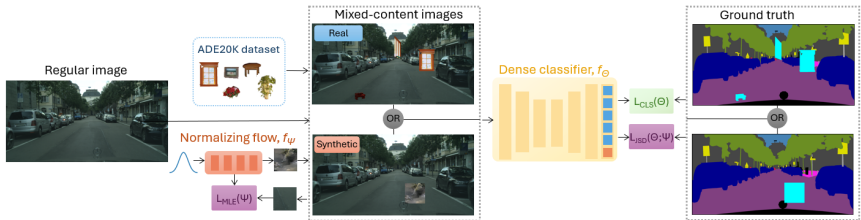


Figure 4: Fine-tuning of dense classifier equipped with UNO. We paste negative training data (either real or synthetic) atop regular inlier images. The resulting mixed-content image is fed to the dense classifier that optimizes cross-entropy loss over K+2 classes.

5 Experiments

Experimental setup. We evaluate the UNO performance on standard image-wide and pixel-level benchmarks. In the pixel-level setup, we consider Fishyscapes [10] and SMIYC [9], the two prominent benchmarks for road driving scenes. In the image-wide setup, we consider the CIFAR-10 and ImageNet-200 setups from the OpenOOD benchmark [102]. We report the standard evaluation metrics AUROC and FPR₉₅ in image-wide, and AP and FPR₉₅ in pixel-level experiments. Our pixel-level experiments start by training the M2F-SwinL [14] on Cityscapes [16] and Vistas [75] with the Cityscapes taxonomy. We extend the mask-wide classifier to K+2 classes and fine-tune on mixed-content images. We compose mixed-content images by pasting negative content (ADE20k [108] instances or flow samples) into inlier images. More implementation details are in the Appendix. Our code is publicly available here¹.

Segmentation of road scenes. Table 1 compares UNO with the related work on Fishyscapes and SMIYC. We observe that mask-level recognition methods outperform earlier works [80, 48, 92]. When training with real negatives, our method outperforms all previous work on Fishyscapes and SMIYC AnomalyTrack, while performing within variance of the best method on SMIYC ObstacleTrack. When training without real negatives, our method outperforms all previous work on SMIYC and Fishyscapes Static by a large margin, while achieving second best AP on Fishyscapes L&F. Interestingly, the inlier recognition performance is not affected by the UNO fine-tuning. The initial closed-set model attains 83.5% mIoU on Cityscapes. Appending UNO and fine-tuning the resulting open-set model with real negatives increases classification performance to 83.7%.

Table 2 compares UNO with previous works that work with mask-level recognition on validation subsets of Fishyscapes and RoadAnomaly [54]. UNO outperforms previous ap-

¹<https://github.com/matejgrcic/Open-set-M2F>

Method	Aux. data	Fishyscapes				SMIYC				Cityscapes
		Lost&Found AP	Found FPR ₉₅	Static AP	Static FPR ₉₅	AnomalyTrack AP	AnomalyTrack FPR ₉₅	ObstacleTrack AP	ObstacleTrack FPR ₉₅	val mIoU
Maximum Entropy [100]	✗	15.0	85.1	0.8	77.9	-	-	-	-	9.7
Image Resynthesis [26]	✗	5.7	48.1	29.6	27.1	52.3	25.9	37.7	4.7	81.4
JSRNet [22]	✗	-	-	-	-	33.6	43.9	28.1	28.9	-
Max softmax [6]	✗	1.8	44.9	12.9	39.8	28.0	72.1	15.7	16.6	80.3
SML [83]	✗	31.7	21.9	52.1	20.5	-	-	-	-	-
Embedding Density [10]	✗	37.5	70.8	0.8	46.4	4.3	47.2	62.1	17.4	80.3
NFlowJS [23]	✗	39.4	9.0	52.1	15.4	-	-	-	-	77.4
SynDHybrid [85]	✗	51.8	11.5	54.7	15.5	-	-	-	-	79.9
cDNP [4]	✗	62.2	8.9	-	-	88.9	11.4	72.70	1.40	-
EAM [†] [10]	✗	9.4	41.5	76.0	10.1	76.3	93.9	66.9	17.9	83.5
RbA [†] [4]	✗	-	-	-	-	86.1	15.9	87.8	3.3	-
Maskomaly [†] [10]	✗	-	-	-	-	93.4	6.9	-	-	-
UNO [†] (ours)	✗	<u>56.4</u>	55.1	91.1	1.5	96.1	2.3	89.0	0.6	83.5
SynBoost [4]	✓	43.2	15.8	72.6	18.8	56.4	61.9	71.3	3.2	81.4
OOD Head [1]	✓	30.9	22.2	84.0	10.3	-	-	-	-	77.3
Void Classifier [10]	✓	10.3	22.1	45.0	19.4	36.6	63.5	10.4	41.5	70.4
Dirichlet prior [10]	✓	34.3	47.4	84.6	30.0	-	-	-	-	70.5
DenseHybrid [80]	✓	43.9	6.2	72.3	5.5	78.0	9.8	78.7	2.1	81.0
PEBAL [85]	✓	44.2	7.6	92.4	1.7	49.1	40.8	5.0	12.7	-
cDNP [4]	✓	69.8	7.5	-	-	88.9	11.4	72.70	1.40	-
RPL [6]	✓	53.9	2.3	95.9	0.5	83.5	11.7	85.9	0.6	-
Mask2Anomaly [†] [45]	✓	46.0	4.4	95.2	0.8	88.7	14.6	93.3	0.2	-
RbA [†] [4]	✓	-	-	-	-	90.9	11.6	91.8	0.5	-
EAM [†] [10]	✓	63.5	39.2	93.6	1.2	93.8	4.1	92.9	0.5	83.5
UNO [†] (ours)	✓	74.8	2.7	95.8	0.3	96.3	2.0	<u>93.2</u>	0.2	83.7

Table 1: Experimental evaluation on the Fishyscapes and SMIYC benchmarks. Methods that leverage mask-level recognition are marked with †. Missing results are marked with -.

proaches across datasets and metrics with the single exception of 0.5 pp worse FPR₉₅ than RbA on RoadAnomaly.

Method	FS L&F		FS Static		RoadAnomaly		FS L&F		FS Static		RoadAnomaly	
	AP	FPR ₉₅	AP	FPR ₉₅	AP	FPR ₉₅	AP	FPR ₉₅	AP	FPR ₉₅	AP	FPR ₉₅
RbA	70.8	6.3	-	-	85.4	6.9	61.0	10.6	-	-	78.5	11.8
Maskomaly	69.4	9.4	90.5	2.0	79.7	13.5	-	-	68.8	15.0	80.8	12.0
EAM	81.5	4.2	96.0	0.3	69.4	7.7	52.0	20.5	87.3	2.1	66.7	13.4
UNO (ours)	81.8	1.3	98.0	0.04	88.5	<u>7.4</u>	74.5	6.9	96.9	0.1	82.4	9.2

Table 2: Validation of mask-level approaches on Fishyscapes val and RoadAnomaly with (left) and without (right) training with real negative data. Missing results are marked with -.

Image classification. Table 3 shows the image-wide performance of UNO on the OpenOOD benchmark [100]. We compare UNO with training methods with and without the use of real negative data. When training with real negatives, UNO consistently outperforms all baselines on CIFAR-10 and near OOD Imagenet-200, while attaining the best AUROC and the second-best FPR on the far OOD Imagenet-200. When training without real negative data, UNO accomplishes competitive performance on both benchmarks. Synthetic UNO outperforms even methods trained with real data, specifically, MixOE, MCD and UDG on CIFAR-10, and UDG on ImageNet-200. It is interesting that UNO trained with synthetic

negatives outperforms UNO trained with real negatives by a significant margin on the far OOD ImageNet-200. Finally, UNO preserves the inlier classification performance.

Method	CIFAR-10					ImageNet-200				
	Near-OOD		Far-OOD		Acc.	Near-OOD		Far-OOD		Acc.
	AUC	FPR	AUC	FPR		AUC	FPR	AUC	FPR	
ConfBranch [14]	89.8	31.3	92.9	94.9	94.9	79.1	61.4	90.4	34.8	85.9
RotPred [14]	92.7	28.1	96.6	12.2	95.4	81.6	60.4	92.6	26.2	86.4
G-ODIN [15]	89.1	45.5	95.5	21.5	94.7	77.3	69.9	92.3	30.2	84.6
CSI [84]	89.5	33.7	92.0	26.4	91.2	-	-	-	-	-
ARPL [10]	87.4	40.3	89.3	32.4	93.7	82.0	55.7	89.2	36.5	84.0
MOS [16]	71.5	78.7	76.4	62.9	94.8	69.8	71.6	80.5	51.6	85.6
VOS [15]	87.7	57.0	90.8	40.4	94.3	82.5	59.9	91.0	34.0	86.2
LogitNorm [19]	92.3	29.3	96.7	13.8	94.3	82.7	56.5	93.0	26.1	86.0
CIDER [17]	90.7	32.1	94.7	20.7	-	80.6	60.1	90.7	30.2	-
NPOS [83]	89.8	32.6	94.1	20.6	-	79.4	62.1	94.5	21.8	-
UNO (ours)	91.3	31.8	92.6	20.5	95.2	81.2	61.1	92.5	32.3	86.3
MixOE [100]	88.7	51.5	91.9	33.8	94.6	82.6	58.0	88.3	40.9	85.7
MCD [12]	91.0	30.2	91.0	32.0	95.0	83.6	54.7	88.9	29.9	86.1
UDG [15]	89.9	35.3	92.4	20.4	92.4	74.3	68.9	82.1	62.0	68.1
OE [83]	94.8	19.8	96.0	13.1	94.6	84.8	52.3	89.0	34.2	85.8
UNO (ours)	94.9	9.3	97.6	9.4	94.9	85.1	51.7	89.6	36.8	86.4

Table 3: OOD detection performance on OpenOOD CIFAR-10 and ImageNet-200. We consider training-based methods with (bottom) and without (top) real negative data. All results were averaged over 3 runs. Full results are available in the Appendix.

Validating components of UNO score. Table 4 validates the contribution of the UNO components. In the case of real negatives, both components attain competitive results while UNO significantly outperforms both of them. In the case of synthetic negatives, uncertainty outperforms the negative objectness by a wide margin. This does not come as a surprise since the negative objectness is inferred from synthetic training negatives. Still, UNO again greatly benefits from the ensemble of the two scores.

Score	FS L&F		FS Static		RoadAnomaly		FS L&F		FS Static		RoadAnomaly	
	AP	FPR ₉₅	AP	FPR ₉₅	AP	FPR ₉₅	AP	FPR ₉₅	AP	FPR ₉₅	AP	FPR ₉₅
UNO	81.8	1.3	98.0	0.04	88.5	7.4	74.5	6.9	96.9	0.1	82.4	9.2
Unc	74.1	4.5	72.1	1.5	66.2	8.0	71.9	8.0	95.7	0.5	70.4	9.4
NO	69.0	1.6	92.6	0.14	80.4	19.8	26.6	91.1	73.9	61.1	54.2	72.3

Table 4: Validation of UNO components with (left) and without (right) real negative data.

Figure 5 visualises UNO performance on FS L&F. Columns show continuous OOD scores and OOD detections after thresholding at 95% TPR. The two UNO components have different failure modes. For example, s_{Unc} produces false positives at the borders of inlier classes while s_{NO} detects some inlier objects as outliers. Still, these failure modes cancel out in the compound UNO score, as designated with green rectangles.

6 Conclusion

Visual recognition models behave unpredictably in presence of outliers. A common strategy to detect outliers is to fine-tune the closed-set classifier in order to increase uncertainty

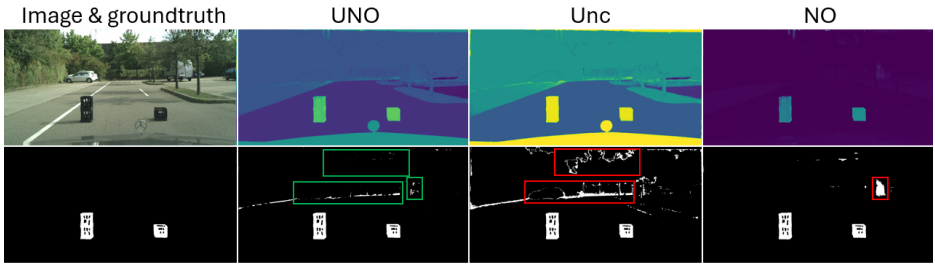


Figure 5: Qualitative experiments on Fishyscapes L&F val. Top row shows the input image and the three outlier scores. Bottom row shows anomaly detection maps after thresholding at TPR=95%. UNO significantly reduces the incidence of false-positive responses.

in negative data. We take a different approach and disentangle the prediction uncertainty from the recognition of outliers. This allows us to cast outlier detection as an ensemble of in-distribution uncertainty and the posterior of the negative class, which we term negative objectness. The resulting UNO score manifests as a lightweight plug-in module that can extend an arbitrary classifier. The resulting model is then fine-tuned with real negative data or their synthetic surrogates. UNO can be applied to per-pixel outlier detection by extending recent mask-level recognition approaches. There we first apply UNO to recover mask-wide outlier scores, and then propagate them to pixels according to mask assignments. UNO attains strong performance on recent image-wide and pixel-level outlier detection benchmarks with and without real negative data. Prominent future developments include improving the quality of synthetic negative data and extending our ensemble with generative predictions.

7 Limitations

Auxiliary training data. UNO relies on negative training data to deliver strong OOD detection performance. While standard applications offer plenty of real negative data, this might not be the case in domain-specific applications such as remote sensing and medical imaging. Still, we show that UNO can deliver strong performance when trained on synthetic negatives.

Confidence calibration. Our $K+1$ -way classifier could be inadequately calibrated which would introduce bias into our uncertainty estimates. An interesting direction for future work is formulation of a better uncertainty estimate.

Acknowledgements

This work has been supported by Croatian Recovery and Resilience Fund - NextGenerationEU (grant C1.4 R5-I2.01.0001), and Croatian Science Foundation (grant IP-2020-02-5851 ADEPT)

References

- [1] Jan Ackermann, Christos Sakaridis, and Fisher Yu. Maskomaly: Zero-shot mask anomaly segmentation. *arXiv preprint arXiv:2305.16972*, 2023.

- [2] Abhijit Bendale and Terrance E. Boult. Towards open set deep networks. In *2016 IEEE Conference on Computer Vision and Pattern Recognition, CVPR 2016, Las Vegas, NV, USA, June 27-30, 2016*, pages 1563–1572. IEEE Computer Society, 2016.
- [3] Petra Bevandić, Ivan Krešo, Marin Oršić, and Siniša Šegvić. Simultaneous semantic segmentation and outlier detection in presence of domain shift. In *41st DAGM German Conference, DAGM GCPR*. Springer, 2019.
- [4] Petra Bevandić, Ivan Krešo, Marin Oršić, and Siniša Šegvić. Dense open-set recognition based on training with noisy negative images. *Image and Vision Computing*, 2022.
- [5] Giancarlo Di Biase, Hermann Blum, Roland Siegart, and César Cadena. Pixel-wise anomaly detection in complex driving scenes. In *IEEE Conference on Computer Vision and Pattern Recognition, CVPR 2021, virtual, June 19-25, 2021*, pages 16918–16927. Computer Vision Foundation / IEEE, 2021. doi: 10.1109/CVPR46437.2021.01664.
- [6] Julian Bitterwolf, Maximilian Müller, and Matthias Hein. In or out? fixing imagenet out-of-distribution detection evaluation. *arXiv preprint arXiv:2306.00826*, 2023.
- [7] Hermann Blum, Paul-Edouard Sarlin, Juan Nieto, Roland Siegart, and Cesar Cadena. The fishyscapes benchmark: Measuring blind spots in semantic segmentation. *International Journal of Computer Vision*, 2021.
- [8] Nicolas Carion, Francisco Massa, Gabriel Synnaeve, Nicolas Usunier, Alexander Kirillov, and Sergey Zagoruyko. End-to-end object detection with transformers. In Andrea Vedaldi, Horst Bischof, Thomas Brox, and Jan-Michael Frahm, editors, *Computer Vision - ECCV 2020 - 16th European Conference, Glasgow, UK, August 23-28, 2020, Proceedings, Part I*, volume 12346 of *Lecture Notes in Computer Science*, pages 213–229. Springer, 2020.
- [9] Robin Chan, Krzysztof Lis, Svenja Uhlemeyer, Hermann Blum, Sina Honari, Roland Siegart, Pascal Fua, Mathieu Salzmann, and Matthias Rottmann. Segmentmeifyoucan: A benchmark for anomaly segmentation. *arXiv preprint arXiv:2104.14812*, 2021.
- [10] Robin Chan, Matthias Rottmann, and Hanno Gottschalk. Entropy maximization and meta classification for out-of-distribution detection in semantic segmentation. In *Proceedings of the IEEE/CVF International Conference on Computer Vision*, pages 5128–5137, 2021.
- [11] Guangyao Chen, Peixi Peng, Xiangqian Wang, and Yonghong Tian. Adversarial reciprocal points learning for open set recognition. *IEEE Trans. Pattern Anal. Mach. Intell.*, 44(11):8065–8081, 2022.
- [12] Liang-Chieh Chen, George Papandreou, Iasonas Kokkinos, Kevin Murphy, and Alan L. Yuille. Deeplab: Semantic image segmentation with deep convolutional nets, atrous convolution, and fully connected crfs. *IEEE Trans. Pattern Anal. Mach. Intell.*, 40(4):834–848, 2018.

- [13] Yiye Chen, Yunzhi Lin, Ruinian Xu, and Patricio A. Vela. Wdiscood: Out-of-distribution detection via whitened linear discriminant analysis. In *IEEE/CVF International Conference on Computer Vision, ICCV 2023, Paris, France, October 1-6, 2023*, pages 5275–5284. IEEE, 2023.
- [14] Bowen Cheng, Ishan Misra, Alexander G Schwing, Alexander Kirillov, and Rohit Girdhar. Masked-attention mask transformer for universal image segmentation. In *Proceedings of the IEEE/CVF conference on computer vision and pattern recognition*, pages 1290–1299, 2022.
- [15] Mircea Cimpoi, Subhansu Maji, Iasonas Kokkinos, Sammy Mohamed, and Andrea Vedaldi. Describing textures in the wild. In *Proceedings of the IEEE conference on computer vision and pattern recognition*, pages 3606–3613, 2014.
- [16] Marius Cordts, Mohamed Omran, Sebastian Ramos, Timo Rehfeld, Markus Enzweiler, Rodrigo Benenson, Uwe Franke, Stefan Roth, and Bernt Schiele. The cityscapes dataset for semantic urban scene understanding. In *Proceedings of the IEEE conference on computer vision and pattern recognition*, pages 3213–3223, 2016.
- [17] Jia Deng, Wei Dong, Richard Socher, Li-Jia Li, Kai Li, and Li Fei-Fei. Imagenet: A large-scale hierarchical image database. In *IEEE Computer Society Conference on Computer Vision and Pattern Recognition CVPR*, 2009.
- [18] Li Deng. The mnist database of handwritten digit images for machine learning research [best of the web]. *IEEE signal processing magazine*, 29(6):141–142, 2012.
- [19] Terrance DeVries and Graham W. Taylor. Learning confidence for out-of-distribution detection in neural networks. *CoRR*, abs/1802.04865, 2018. URL <http://arxiv.org/abs/1802.04865>.
- [20] Akshay Raj Dhamija, Manuel Günther, and Terrance E. Boult. Reducing network agnostophobia. In *Proceedings of the 32nd International Conference on Neural Information Processing Systems, NIPS’18*, page 9175–9186, 2018.
- [21] Giancarlo Di Biase, Hermann Blum, Roland Siegwart, and Cesar Cadena. Pixel-wise anomaly detection in complex driving scenes. In *Proceedings of the IEEE/CVF conference on computer vision and pattern recognition*, pages 16918–16927, 2021.
- [22] Laurent Dinh, Jascha Sohl-Dickstein, and Samy Bengio. Density estimation using real NVP. In *International Conference on Learning Representations*, 2017.
- [23] Andrija Djuricic, Nebojsa Bozanic, Arjun Ashok, and Rosanne Liu. Extremely simple activation shaping for out-of-distribution detection. *arXiv preprint arXiv:2209.09858*, 2022.
- [24] Alexey Dosovitskiy, Lucas Beyer, Alexander Kolesnikov, Dirk Weissenborn, Xiaohua Zhai, Thomas Unterthiner, Mostafa Dehghani, Matthias Minderer, Georg Heigold, Sylvain Gelly, Jakob Uszkoreit, and Neil Houlsby. An image is worth 16x16 words: Transformers for image recognition at scale. In *International Conference on Learning Representations, ICLR*, 2021.

- [25] Xuefeng Du, Zhaoning Wang, Mu Cai, and Yixuan Li. VOS: learning what you don't know by virtual outlier synthesis. In *The Tenth International Conference on Learning Representations, ICLR*, 2022.
- [26] Silvio Galesso, Max Argus, and Thomas Brox. Far away in the deep space: Nearest-neighbor-based dense out-of-distribution detection. *CoRR*, abs/2211.06660, 2022. doi: 10.48550/ARXIV.2211.06660. URL <https://doi.org/10.48550/arXiv.2211.06660>.
- [27] Matej Grcić, Petra Bevandić, and Siniša Šegvić. Dense anomaly detection by robust learning on synthetic negative data. *arXiv preprint arXiv:2112.12833*, 2021.
- [28] Matej Grcić, Petra Bevandić, and Siniša Šegvić. Dense open-set recognition with synthetic outliers generated by real nvp. In *16th International Joint Conference on Computer Vision, Imaging and Computer Graphics Theory and Applications, VISIGRAPP*, 2021.
- [29] Matej Grcić, Ivan Grubišić, and Siniša Šegvić. Densely connected normalizing flows. *Advances in Neural Information Processing Systems*, 2021.
- [30] Matej Grcic, Petra Bevanđic, and Sinisa Segvic. Densehybrid: Hybrid anomaly detection for dense open-set recognition. In *European Conference on Computer Vision, ECCV 2022*. Springer, 2022.
- [31] Matej Grcić, Josip Šarić, and Siniša Šegvić. On advantages of mask-level recognition for outlier-aware segmentation. In *Proceedings of the IEEE/CVF Conference on Computer Vision and Pattern Recognition*, pages 2936–2946, 2023.
- [32] Matej Grcic, Petra Bevanđic, Zoran Kalafatic, and Sinisa Segvic. Dense out-of-distribution detection by robust learning on synthetic negative data. *Sensors*, 24(4): 1248, 2024.
- [33] Matej Grcić and Siniša Šegvić. Hybrid open-set segmentation with synthetic negative data. *IEEE Transactions on Pattern Analysis and Machine Intelligence*, 2024.
- [34] Matej Grcić and Siniša Šegvić. Hybrid open-set segmentation with synthetic negative data. *IEEE Transactions on Pattern Analysis and Machine Intelligence*, 2024.
- [35] Chuan Guo, Geoff Pleiss, Yu Sun, and Kilian Q Weinberger. On calibration of modern neural networks. In *International conference on machine learning*, pages 1321–1330. PMLR, 2017.
- [36] Kaiming He, Xiangyu Zhang, Shaoqing Ren, and Jian Sun. Deep residual learning for image recognition. In *Proceedings of the IEEE conference on computer vision and pattern recognition*, pages 770–778, 2016.
- [37] Dan Hendrycks and Kevin Gimpel. A baseline for detecting misclassified and out-of-distribution examples in neural networks. *arXiv preprint arXiv:1610.02136*, 2016.
- [38] Dan Hendrycks and Kevin Gimpel. A baseline for detecting misclassified and out-of-distribution examples in neural networks. In *5th International Conference on Learning Representations, ICLR 2017, Toulon, France, April 24-26, 2017, Conference Track Proceedings*. OpenReview.net, 2017.

- [39] Dan Hendrycks, Mantas Mazeika, and Thomas Dietterich. Deep anomaly detection with outlier exposure. *arXiv preprint arXiv:1812.04606*, 2018.
- [40] Dan Hendrycks, Steven Basart, Mantas Mazeika, Andy Zou, Joe Kwon, Mohammadreza Mostajabi, Jacob Steinhardt, and Dawn Song. Scaling out-of-distribution detection for real-world settings. *arXiv preprint arXiv:1911.11132*, 2019.
- [41] Dan Hendrycks, Mantas Mazeika, Saurav Kadavath, and Dawn Song. Using self-supervised learning can improve model robustness and uncertainty. *Advances in neural information processing systems*, 32, 2019.
- [42] Dan Hendrycks, Steven Basart, Mantas Mazeika, Andy Zou, Joe Kwon, Mohammadreza Mostajabi, Jacob Steinhardt, and Dawn Song. Scaling out-of-distribution detection for real-world settings. *ICML*, 2022.
- [43] Dan Hendrycks, Steven Basart, Mantas Mazeika, Andy Zou, Joseph Kwon, Mohammadreza Mostajabi, Jacob Steinhardt, and Dawn Song. Scaling out-of-distribution detection for real-world settings. In Kamalika Chaudhuri, Stefanie Jegelka, Le Song, Csaba Szepesvári, Gang Niu, and Sivan Sabato, editors, *International Conference on Machine Learning, ICML 2022, 17-23 July 2022, Baltimore, Maryland, USA*, volume 162 of *Proceedings of Machine Learning Research*, pages 8759–8773. PMLR, 2022.
- [44] Geoffrey E. Hinton, Oriol Vinyals, and Jeffrey Dean. Distilling the knowledge in a neural network. *CoRR*, abs/1503.02531, 2015.
- [45] Yen-Chang Hsu, Yilin Shen, Hongxia Jin, and Zsolt Kira. Generalized ODIN: detecting out-of-distribution image without learning from out-of-distribution data. In *2020 IEEE/CVF Conference on Computer Vision and Pattern Recognition, CVPR 2020, Seattle, WA, USA, June 13-19, 2020*, pages 10948–10957. Computer Vision Foundation / IEEE, 2020.
- [46] Rui Huang and Yixuan Li. MOS: towards scaling out-of-distribution detection for large semantic space. In *IEEE Conference on Computer Vision and Pattern Recognition, CVPR 2021, virtual, June 19-25, 2021*, pages 8710–8719. Computer Vision Foundation / IEEE, 2021.
- [47] Rui Huang, Andrew Geng, and Yixuan Li. On the importance of gradients for detecting distributional shifts in the wild. In Marc’Aurelio Ranzato, Alina Beygelzimer, Yann N. Dauphin, Percy Liang, and Jennifer Wortman Vaughan, editors, *Advances in Neural Information Processing Systems 34: Annual Conference on Neural Information Processing Systems 2021, NeurIPS 2021, December 6-14, 2021, virtual*, pages 677–689, 2021.
- [48] Sanghun Jung, Jungsoo Lee, Daehoon Gwak, Sungha Choi, and Jaegul Choo. Standardized max logits: A simple yet effective approach for identifying unexpected road obstacles in urban-scene segmentation. In *Proceedings of the IEEE/CVF International Conference on Computer Vision*, pages 15425–15434, 2021.
- [49] Diederik P. Kingma and Prafulla Dhariwal. Glow: Generative flow with invertible 1x1 convolutions. In *Advances in Neural Information Processing Systems 31: Annual Conference on Neural Information Processing Systems 2018, NeurIPS 2018*, 2018.

- [50] Shu Kong and Deva Ramanan. Opegan: Open-set recognition via open data generation. In *2021 IEEE/CVF International Conference on Computer Vision, ICCV 2021, Montreal, QC, Canada, October 10-17, 2021*, pages 793–802. IEEE, 2021.
- [51] Alex Krizhevsky. Learning multiple layers of features from tiny images. Technical report, University of Toronto, 2009.
- [52] Alex Krizhevsky, Vinod Nair, and Geoffrey Hinton. Cifar-10 and cifar-100 datasets. URL: <https://www.cs.toronto.edu/kriz/cifar.html>, 6(1):1, 2009.
- [53] Nishant Kumar, Sinisa Segvic, Abouzar Eslami, and Stefan Gumhold. Normalizing flow based feature synthesis for outlier-aware object detection. In *IEEE/CVF Conference on Computer Vision and Pattern Recognition, CVPR 2023, Vancouver, BC, Canada, June 17-24, 2023*, pages 5156–5165. IEEE, 2023.
- [54] L. I. Kuncheva and C. J. Whitaker. Measures of diversity in classifier ensembles and their relationship with the ensemble accuracy. *Machine Learning*, 2003.
- [55] Balaji Lakshminarayanan, Alexander Pritzel, and Charles Blundell. Simple and scalable predictive uncertainty estimation using deep ensembles. *Advances in neural information processing systems*, 30, 2017.
- [56] Ya Le and Xuan Yang. Tiny imagenet visual recognition challenge. *CS 231N*, 7(7):3, 2015.
- [57] Kimin Lee, Honglak Lee, Kibok Lee, and Jinwoo Shin. Training confidence-calibrated classifiers for detecting out-of-distribution samples. In *International Conference on Learning Representations*, 2018.
- [58] Kimin Lee, Kibok Lee, Honglak Lee, and Jinwoo Shin. A simple unified framework for detecting out-of-distribution samples and adversarial attacks. In Samy Bengio, Hanna M. Wallach, Hugo Larochelle, Kristen Grauman, Nicolò Cesa-Bianchi, and Roman Garnett, editors, *Advances in Neural Information Processing Systems 31: Annual Conference on Neural Information Processing Systems 2018, NeurIPS 2018, December 3-8, 2018, Montréal, Canada*, pages 7167–7177, 2018.
- [59] Feng Li, Hao Zhang, Huaizhe xu, Shilong Liu, Lei Zhang, Lionel M. Ni, and Heung-Yeung Shum. Mask dino: Towards a unified transformer-based framework for object detection and segmentation. In *CVPR*, 2023.
- [60] Chen Liang, Wenguan Wang, Jiaxu Miao, and Yi Yang. Gmmseg: Gaussian mixture based generative semantic segmentation models. In Sanmi Koyejo, S. Mohamed, A. Agarwal, Danielle Belgrave, K. Cho, and A. Oh, editors, *Advances in Neural Information Processing Systems 35: Annual Conference on Neural Information Processing Systems 2022, NeurIPS 2022, New Orleans, LA, USA, November 28 - December 9, 2022*, 2022.
- [61] Shiyu Liang, Yixuan Li, and Rayadurgam Srikant. Enhancing the reliability of out-of-distribution image detection in neural networks. *arXiv preprint arXiv:1706.02690*, 2017.

- [62] Tsung-Yi Lin, Michael Maire, Serge Belongie, James Hays, Pietro Perona, Deva Ramanan, Piotr Dollár, and C Lawrence Zitnick. Microsoft coco: Common objects in context. In *Computer Vision–ECCV 2014: 13th European Conference, Zurich, Switzerland, September 6-12, 2014, Proceedings, Part V 13*, pages 740–755. Springer, 2014.
- [63] Tsung-Yi Lin, Michael Maire, Serge J. Belongie, James Hays, Pietro Perona, Deva Ramanan, Piotr Dollár, and C. Lawrence Zitnick. Microsoft COCO: common objects in context. In *13th European Conference of Computer Vision ECCV*. Springer, 2014.
- [64] Krzysztof Lis, Krishna Nakka, Pascal Fua, and Mathieu Salzmann. Detecting the unexpected via image resynthesis. In *Proceedings of the IEEE/CVF International Conference on Computer Vision*, pages 2152–2161, 2019.
- [65] Weitang Liu, Xiaoyun Wang, John D. Owens, and Yixuan Li. Energy-based out-of-distribution detection. In Hugo Larochelle, Marc’Aurelio Ranzato, Raia Hadsell, Maria-Florina Balcan, and Hsuan-Tien Lin, editors, *Advances in Neural Information Processing Systems 33: Annual Conference on Neural Information Processing Systems 2020, NeurIPS 2020, December 6-12, 2020, virtual*, 2020.
- [66] Yuyuan Liu, Choubo Ding, Yu Tian, Guansong Pang, Vasileios Belagiannis, Ian D. Reid, and Gustavo Carneiro. Residual pattern learning for pixel-wise out-of-distribution detection in semantic segmentation. In *IEEE/CVF International Conference on Computer Vision, ICCV 2023, Paris, France, October 1-6, 2023*, pages 1151–1161. IEEE, 2023.
- [67] Ze Liu, Yutong Lin, Yue Cao, Han Hu, Yixuan Wei, Zheng Zhang, Stephen Lin, and Baining Guo. Swin transformer: Hierarchical vision transformer using shifted windows. In *Proceedings of the IEEE/CVF international conference on computer vision*, pages 10012–10022, 2021.
- [68] Zhuang Liu, Hanzi Mao, Chao-Yuan Wu, Christoph Feichtenhofer, Trevor Darrell, and Saining Xie. A convnet for the 2020s. In *IEEE/CVF Conference on Computer Vision and Pattern Recognition, CVPR 2022, New Orleans, LA, USA, June 18-24, 2022*, 2022.
- [69] Thomas Lucas, Konstantin Shmelkov, Karteek Alahari, Cordelia Schmid, and Jakob Verbeek. Adaptive density estimation for generative models. In Hanna M. Wallach, Hugo Larochelle, Alina Beygelzimer, Florence d’Alché-Buc, Emily B. Fox, and Roman Garnett, editors, *Advances in Neural Information Processing Systems 32: Annual Conference on Neural Information Processing Systems 2019, NeurIPS 2019, December 8-14, 2019, Vancouver, BC, Canada*, pages 11993–12003, 2019.
- [70] Andrey Malinin and Mark Gales. Predictive uncertainty estimation via prior networks. *Advances in neural information processing systems*, 31, 2018.
- [71] Yifei Ming, Yiyu Sun, Ousmane Dia, and Yixuan Li. How to exploit hyperspherical embeddings for out-of-distribution detection? In *The Eleventh International Conference on Learning Representations, ICLR 2023, Kigali, Rwanda, May 1-5, 2023*. OpenReview.net, 2023.

- [72] Jishnu Mukhoti and Yarin Gal. Evaluating bayesian deep learning methods for semantic segmentation. *arXiv preprint arXiv:1811.12709*, 2018.
- [73] Nazir Nayal, Misra Yavuz, Joao F Henriques, and Fatma Güney. Rba: Segmenting unknown regions rejected by all. In *Proceedings of the IEEE/CVF International Conference on Computer Vision*, pages 711–722, 2023.
- [74] Lawrence Neal, Matthew Olson, Xiaoli Fern, Weng-Keen Wong, and Fuxin Li. Open set learning with counterfactual images. In *Proceedings of the European Conference on Computer Vision (ECCV)*, 2018.
- [75] Gerhard Neuhold, Tobias Ollmann, Samuel Rota Buló, and Peter Kotschieder. The mapillary vistas dataset for semantic understanding of street scenes. In *Proceedings of the IEEE international conference on computer vision*, pages 4990–4999, 2017.
- [76] SoonCheol Noh, DongEon Jeong, and Jee-Hyong Lee. Simple and effective out-of-distribution detection via cosine-based softmax loss. In *IEEE/CVF International Conference on Computer Vision, ICCV 2023, Paris, France, October 1-6, 2023*, pages 16514–16523. IEEE, 2023.
- [77] Jaewoo Park, Yoon Gyo Jung, and Andrew Beng Jin Teoh. Nearest neighbor guidance for out-of-distribution detection. In *IEEE/CVF International Conference on Computer Vision, ICCV 2023, Paris, France, October 1-6, 2023*, pages 1686–1695. IEEE, 2023.
- [78] Shyam Nandan Rai, Fabio Cermelli, Dario Fontanel, Carlo Masone, and Barbara Caputo. Unmasking anomalies in road-scene segmentation. In *Proceedings of the IEEE/CVF International Conference on Computer Vision*, pages 4037–4046, 2023.
- [79] Jie Ren, Stanislav Fort, Jeremiah Z. Liu, Abhijit Guha Roy, Shreyas Padhy, and Balaji Lakshminarayanan. A simple fix to mahalanobis distance for improving near-ood detection. *CoRR*, abs/2106.09022, 2021.
- [80] Lukas Ruff, Jacob R. Kauffmann, Robert A. Vandermeulen, Grégoire Montavon, Wojciech Samek, Marius Kloft, Thomas G. Dietterich, and Klaus-Robert Müller. A unifying review of deep and shallow anomaly detection. *Proc. IEEE*, 109(5):756–795, 2021.
- [81] Chandramouli Shama Sastry and Sageev Oore. Detecting out-of-distribution examples with gram matrices. In *Proceedings of the 37th International Conference on Machine Learning, ICML 2020, 13-18 July 2020, Virtual Event*, volume 119 of *Proceedings of Machine Learning Research*, pages 8491–8501. PMLR, 2020.
- [82] Yue Song, Nicu Sebe, and Wei Wang. Rankfeat: Rank-1 feature removal for out-of-distribution detection. In Sanmi Koyejo, S. Mohamed, A. Agarwal, Danielle Belgrave, K. Cho, and A. Oh, editors, *Advances in Neural Information Processing Systems 35: Annual Conference on Neural Information Processing Systems 2022, NeurIPS 2022, New Orleans, LA, USA, November 28 - December 9, 2022*, 2022.
- [83] Yiyou Sun and Yixuan Li. DICE: leveraging sparsification for out-of-distribution detection. In Shai Avidan, Gabriel J. Brostow, Moustapha Cissé, Giovanni Maria Farinella, and Tal Hassner, editors, *Computer Vision - ECCV 2022: 17th European Conference, Tel Aviv, Israel, October 23-27, 2022, Proceedings, Part XXIV*, volume 13684 of *Lecture Notes in Computer Science*, pages 691–708. Springer, 2022.

- [84] Yiyou Sun, Chuan Guo, and Yixuan Li. React: Out-of-distribution detection with rectified activations. In Marc’Aurelio Ranzato, Alina Beygelzimer, Yann N. Dauphin, Percy Liang, and Jennifer Wortman Vaughan, editors, *Advances in Neural Information Processing Systems 34: Annual Conference on Neural Information Processing Systems 2021, NeurIPS 2021, December 6-14, 2021, virtual*, pages 144–157, 2021.
- [85] Yiyou Sun, Yifei Ming, Xiaojin Zhu, and Yixuan Li. Out-of-distribution detection with deep nearest neighbors. In Kamalika Chaudhuri, Stefanie Jegelka, Le Song, Csaba Szepesvári, Gang Niu, and Sivan Sabato, editors, *International Conference on Machine Learning, ICML 2022, 17-23 July 2022, Baltimore, Maryland, USA*, volume 162 of *Proceedings of Machine Learning Research*, pages 20827–20840. PMLR, 2022.
- [86] Jihoon Tack, Sangwoo Mo, Jongheon Jeong, and Jinwoo Shin. CSI: novelty detection via contrastive learning on distributionally shifted instances. In *Advances in Neural Information Processing Systems 33: Annual Conference on Neural Information Processing Systems 2020, NeurIPS 2020, December 6-12, 2020, virtual*, 2020.
- [87] Masoud Taghikhah, Nishant Kumar, Sinisa Segvic, Abouzar Eslami, and Stefan Gumhold. Quantile-based maximum likelihood training for outlier detection. In Michael J. Wooldridge, Jennifer G. Dy, and Sriraam Natarajan, editors, *Thirty-Eighth AAAI Conference on Artificial Intelligence, AAAI 2024, Thirty-Sixth Conference on Innovative Applications of Artificial Intelligence, IAAI 2024, Fourteenth Symposium on Educational Advances in Artificial Intelligence, EAAI 2014, February 20-27, 2024, Vancouver, Canada*, pages 21610–21618. AAAI Press, 2024.
- [88] Leitian Tao, Xuefeng Du, Jerry Zhu, and Yixuan Li. Non-parametric outlier synthesis. In *The Eleventh International Conference on Learning Representations, ICLR, 2023*.
- [89] Yu Tian, Yuyuan Liu, Guansong Pang, Fengbei Liu, Yuanhong Chen, and Gustavo Carneiro. Pixel-wise energy-biased abstention learning for anomaly segmentation on complex urban driving scenes. In *European Conference on Computer Vision*, pages 246–263. Springer, 2022.
- [90] Grant Van Horn, Oisín Mac Aodha, Yang Song, Yin Cui, Chen Sun, Alex Shepard, Hartwig Adam, Pietro Perona, and Serge Belongie. The inaturalist species classification and detection dataset. In *Proceedings of the IEEE conference on computer vision and pattern recognition*, pages 8769–8778, 2018.
- [91] Sagar Vaze, Kai Han, Andrea Vedaldi, and Andrew Zisserman. Open-set recognition: A good closed-set classifier is all you need? *arXiv preprint arXiv:2110.06207*, 2021.
- [92] Tomas Vojir, Tomáš Šipka, Rahaf Aljundi, Nikolay Chumerin, Daniel Olmeda Reino, and Jiri Matas. Road anomaly detection by partial image reconstruction with segmentation coupling. In *Proceedings of the IEEE/CVF International Conference on Computer Vision*, pages 15651–15660, 2021.
- [93] Haoqi Wang, Zhizhong Li, Litong Feng, and Wayne Zhang. Vim: Out-of-distribution with virtual-logit matching. In *Proceedings of the IEEE/CVF conference on computer vision and pattern recognition*, pages 4921–4930, 2022.

- [94] Hongxin Wei, Renchunzi Xie, Hao Cheng, Lei Feng, Bo An, and Yixuan Li. Mitigating neural network overconfidence with logit normalization. In *International Conference on Machine Learning, ICML 2022, 17-23 July 2022*, volume 162 of *Proceedings of Machine Learning Research*, pages 23631–23644. PMLR, 2022.
- [95] Jingkang Yang, Haoqi Wang, Litong Feng, Xiaopeng Yan, Huabin Zheng, Wayne Zhang, and Ziwei Liu. Semantically coherent out-of-distribution detection. In *Proceedings of the IEEE/CVF International Conference on Computer Vision*, pages 8301–8309, 2021.
- [96] Qihang Yu, Huiyu Wang, Siyuan Qiao, Maxwell Collins, Yukun Zhu, Hartwig Adam, Alan Yuille, and Liang-Chieh Chen. k-means Mask Transformer. In *ECCV, 2022*.
- [97] Qing Yu and Kiyoharu Aizawa. Unsupervised out-of-distribution detection by maximum classifier discrepancy. In *Proceedings of the IEEE/CVF international conference on computer vision*, pages 9518–9526, 2019.
- [98] Netzer Yuval. Reading digits in natural images with unsupervised feature learning. In *Proceedings of the NIPS Workshop on Deep Learning and Unsupervised Feature Learning*, 2011.
- [99] Oliver Zendel, Katrin Honauer, Markus Murschitz, Daniel Steiningger, and Gustavo Fernández Domínguez. Wilddash - creating hazard-aware benchmarks. In Vittorio Ferrari, Martial Hebert, Cristian Sminchisescu, and Yair Weiss, editors, *Computer Vision - ECCV 2018 - 15th European Conference, Munich, Germany, September 8-14, 2018, Proceedings, Part VI*, volume 11210 of *Lecture Notes in Computer Science*, pages 407–421. Springer, 2018. URL https://doi.org/10.1007/978-3-030-01231-1_25.
- [100] Hongjie Zhang, Ang Li, Jie Guo, and Yanwen Guo. Hybrid models for open set recognition. In Andrea Vedaldi, Horst Bischof, Thomas Brox, and Jan-Michael Frahm, editors, *Computer Vision - ECCV 2020 - 16th European Conference, Glasgow, UK, August 23-28, 2020, Proceedings, Part III*, volume 12348 of *Lecture Notes in Computer Science*, pages 102–117. Springer, 2020.
- [101] Jingyang Zhang, Nathan Inkawhich, Randolph Linderman, Yiran Chen, and Hai Li. Mixture outlier exposure: Towards out-of-distribution detection in fine-grained environments. In *Proceedings of the IEEE/CVF Winter Conference on Applications of Computer Vision*, pages 5531–5540, 2023.
- [102] Jingyang Zhang, Jingkang Yang, Pengyun Wang, Haoqi Wang, Yueqian Lin, Hao-ran Zhang, Yiyou Sun, Xuefeng Du, Kaiyang Zhou, Wayne Zhang, et al. Openood v1. 5: Enhanced benchmark for out-of-distribution detection. *arXiv preprint arXiv:2306.09301*, 2023.
- [103] Jinsong Zhang, Qiang Fu, Xu Chen, Lun Du, Zelin Li, Gang Wang, Shi Han, Dongmei Zhang, et al. Out-of-distribution detection based on in-distribution data patterns memorization with modern hopfield energy. In *The Eleventh International Conference on Learning Representations*, 2022.

- [104] Jinsong Zhang, Qiang Fu, Xu Chen, Lun Du, Zelin Li, Gang Wang, Xiaoguang Liu, Shi Han, and Dongmei Zhang. Out-of-distribution detection based on in-distribution data patterns memorization with modern hopfield energy. In *The Eleventh International Conference on Learning Representations, ICLR 2023, Kigali, Rwanda, May 1-5, 2023*. OpenReview.net, 2023.
- [105] Zhilin Zhao, Longbing Cao, and Kun-Yu Lin. Revealing distributional vulnerability of explicit discriminators by implicit generators. *CoRR*, 2021.
- [106] Bolei Zhou, Agata Lapedriza, Aditya Khosla, Aude Oliva, and Antonio Torralba. Places: A 10 million image database for scene recognition. *IEEE transactions on pattern analysis and machine intelligence*, 40(6):1452–1464, 2017.
- [107] Bolei Zhou, Hang Zhao, Xavier Puig, Sanja Fidler, Adela Barriuso, and Antonio Torralba. Scene parsing through ade20k dataset. In *Proceedings of the IEEE conference on computer vision and pattern recognition*, 2017.
- [108] Bolei Zhou, Hang Zhao, Xavier Puig, Tete Xiao, Sanja Fidler, Adela Barriuso, and Antonio Torralba. Semantic understanding of scenes through the ade20k dataset. *International Journal of Computer Vision*, 127:302–321, 2019.

A Correlation analysis of UNO components

Table 5 reports the Pearson correlation coefficient of per-pixel outlier scores s_{Unc} and s_{NO} on Fishyscapes [4] val and RoadAnomaly [62]. We observe that the two UNO components are either mildly correlated or completely uncorrelated. These findings indicate that the performance gains of UNO can be explained by the ensemble learning [62].

Data	FS L&F	FS Static	RoadAnomaly
Outliers	0.27	0.01	0.13
Inliers	0.01	0.15	0.01
All	0.16	0.56	0.41

Table 5: Pearson correlation coefficient of per-pixel scores s_{Unc} and s_{NO} on the three outlier segmentation validation datasets (FS L&F, FS Static and RoadAnomaly).

The benefits of ensembling can also be observed in the feature space. Figure 6 indicates that features from different outlier datasets have different L_2 norms. Outliers that resemble the training negatives typically have a higher norm and small angle to \mathbf{w}_{K+1} , while outliers that are more similar to inliers have lower norm. In the former case, outliers are detected with s_{NO} and with s_{Unc} in the latter case.

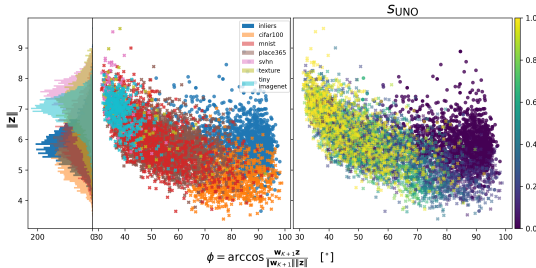


Figure 6: Visualization of the pre-logit space for OpenOOD CIFAR-10. Outlier feature representations either yield an above-average norm with a small angle to \mathbf{w}_{K+1} (e.g. SVHN and Places365) or yield low norm representations (e.g. CIFAR-100 that is similar to inliers).

B On orthogonality of class vectors

We empirically observe that all class vectors \mathbf{w}_i are mutually orthogonal to each other, $\mathbf{w}_i^T \mathbf{w}_j = 0, \forall i, j \in \{1, 2, \dots, K+1\}$, as shown in Figure 7. The cosine of the angle between any two different class vectors is approximately zero. Such behaviour allows the geometrical interpretation of UNO, as shown in Figure 2 of the main manuscript.

C Scene parsing with mask-wide recognition

We extend the Mask2Former [4] architecture with our UNO outlier detector to solve the task of anomaly segmentation. Thus, we describe Mask2Former architecture in detail to make the manuscript self-contained. The Mask2Former architecture consists of three main parts: backbone, pixel decoder, and mask decoder. The backbone extracts features at multiple

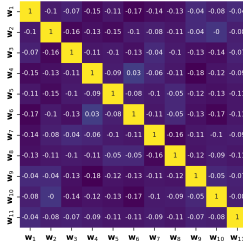


Figure 7: We show that all weight vectors are mutually orthogonal in the form of a heatmap where each element shows the cosine of the angle between two corresponding weight vectors. We use the K+1-way image-wide classifier with the ResNet-18 backbone trained on CIFAR-10 as the example.

scales from a given image $\mathbf{x} \in \mathbb{R}^{3 \times H \times W}$. The pixel decoder produces high-resolution per-pixel features $\mathbf{E} \in \mathbb{R}^{E \times H \times W}$ that are fed into the mask decoder. The mask decoder formulates semantic segmentation as a direct set prediction problem by providing two outputs: N mask embeddings \mathbf{q} , and N mask-wide categorical distributions over $K+1$ classes $P(Y = k | \mathbf{z}_i) = \text{softmax}(\mathbf{W} \cdot \mathbf{z}_i + \mathbf{b})$. The $K+1$ classes include K inlier classes and one no-object class. Note that \mathbf{z}_i denotes the vector of mask-wide pre-logit activations of the i -th mask. The mask decoder projects pre-logits \mathbf{z}_i into logits by applying the learned matrix \mathbf{W} . The binary masks $\mathbf{m} = \sigma(\text{conv}_{1 \times 1}(\mathbf{E}, \mathbf{q}))$ are obtained by scoring per-pixel features \mathbf{E} with the mask embeddings \mathbf{q} . The sigmoid activation interprets each element of the obtained tensor as a probabilistic assignment of the particular pixel into the corresponding mask. Semantic segmentation can be carried out by classifying each pixel according to a weighted ensemble of per-mask classifiers $P(y | \mathbf{z})$, where the weights correspond to dense mask assignments \mathbf{m} :

$$\hat{y}[r, c] = \underset{k=1, \dots, K}{\operatorname{argmax}} \sum_i^N \mathbf{m}_i[r, c] P(Y = k | \mathbf{z}_i). \quad (7)$$

Default mask-level posterior already includes $K+1$ classes that correspond to K inlier classes and one no-object class. We implement our method by introducing an additional class to learn the negative objectness, which brings us to $K+2$ classes in total. To be consistent with the image-wide setup, in addition to the K inlier classes, we place the outlier class at index $K+1$ and the no-object class at index $K+2$. We expose the segmentation model to negative data by training on mixed-content images [10]. Closed-set recognition can still be carried out by considering only the K inlier logits (7).

We detect anomalies on the mask-level by applying UNO to the mask-wide pre-logits \mathbf{z}_i of the i -th mask. We define the per-pixel outlier score at spatial positions r and c as a sum of mask-level outlier scores weighted with dense probabilistic mask assignments [5]:

$$\mathbf{s}_{\text{UNO}}^{\text{M2F}}[r, c] = \sum_{i=1}^N \mathbf{m}_i[r, c] \cdot \mathbf{s}_{\text{UNO}}(\mathbf{z}_i). \quad (8)$$

D Experimental setup

D.1 Benchmarks and datasets

We evaluate UNO on pixel-level outlier detection benchmarks Fishyscapes [7] and SMIYC [9] and the image-wide OpenOOD [10] benchmark.

Pixel-level benchmarks. Fishyscapes [7] contains datasets with real (FS Lost&Found) and synthetic (FS Static) outliers. SMIYC [9] has two dominant tracks which group anomalies according to size. AnomalyTrack focuses on the detection of large anomalies on the traffic scenes while ObstacleTrack focuses on the detection of small obstacles on the road. Additionally, we validate on the RoadAnomaly [6] dataset which is an early version of the AnomalyTrack dataset.

Image-level benchmarks. OpenOOD [10] proposed a unified benchmark for image-wide OOD detection with large-scale datasets. The test outliers are divided into two groups (Near-OOD and Far-OOD) based on semantical similarity to the inlier classes or observed empirical difficulty. The far-OOD group consists of outliers that are semantically far from the inliers (numerical digits, textural patterns, or scene imagery). The near-OOD group consists of outliers that are semantically similar to the inliers as they all include specific objects. The OpenOOD-CIFAR-10 setup uses the official CIFAR-10 [5] splits as ID train, val and test subsets. The negative dataset corresponds to a subset of Tiny ImageNet (TIN) [6]. The near-OOD datasets include CIFAR-100 [5] and a subset of Tiny ImageNet (TIN) [6] that does not overlap with CIFAR-10 and the negative dataset. The far-OOD group consists of MNIST [8], SVHN [9], Textures [4], and Places365 [10] without images that are related with any of the ID classes. The large-scale OpenOOD ImageNet-200 benchmark considers a subset of 200 classes from ImageNet-1K [1] as the inlier training dataset. The remaining 800 classes are used as the negative dataset. The near-OOD group consists of SSB-hard [9] and NINCO [8] while the far-OOD group includes iNaturalist [9], Textures [4], and OpenImage-O [9].

D.2 Evaluation metrics

We use standard evaluation metrics: area under the precision-recall curve (AP), area under the receiver operating curve (AUROC or AUC), and false positive rate at 95% true positive rate (FPR₉₅). We validate in-distribution performance with accuracy and mIoU. Note that we omit the AUROC metric in the pixel-level experiments since all methods achieve high AUROC within variance.

D.3 Implementation details

Segmentation of road scenes. Our pixel-level experiments build upon a Mask2Former model [4] with an ImageNet-initialized SWIN-L [6] backbone. We pre-train the Mask2Former in closed-set setup for 115K iterations on Cityscapes [11] and Mapillary Vistas [12] with the Cityscapes taxonomy. We use the default hyperparameters [4] and set the batch size to 18. We extend the mask-wide classifier to K+2 classes and fine-tune the model on mixed-content scenes with either real or synthetic negatives for 2K iterations. We use the zero-initialization for the added weights. When training with real negative data, we assemble mixed-content images by pasting three semantically different instances sampled from ADE20K [13] after resizing to the range of [96, 512]. In the case of training with synthetic negatives, we

jointly fine tune the K+2-way segmentation model and a flow by adding the loss defined in Equation 6 in the main manuscript to the standard optimization process [44]. We use the DenseFlow-25-6 [49] that we pretrain on Mapillary Vistas for 300 epochs. We generate rectangular patches with spatial dimensions in the range of [48, 512] by sampling the jointly trained flow. We set the loss modulation parameter from Equation 6 to 0.03. We find that training our segmentation model with negatives from scratch, besides from being computationally expensive, leads to overfitting to negatives. Thus, we only finetune the model trained in closed-set manner with both real and synthetic negatives. Additionally, in this case we do not observe feature collapse when utilizing the joint loss (Equation 6 in the main manuscript) since we only jointly train for a small number of iterations. The closed-set training of Mask2Former lasts 48 hours, while the fine-tuning stage takes only 30 minutes on three A6000 GPUs.

Image classification Our image-wide experiments follow the official training setup [102]. When training with real negatives, we train the ResNet-18 [56] backbone with a K+1-way classification layer for 100 epochs from random initialization. We use the SGD optimizer with a momentum of 0.9 and a learning rate of 0.1 with cosine annealing decay schedule. We apply the weight decay of 0.0005. We set the batch size to 128 for CIFAR-10 and 256 for ImageNet-200. Each minibatch contains the equal ratio of all K+1 classes. Specifically, for CIFAR-10 the minibatch contains 117 inlier images and 11 negative images, and 255 inliers and only one negative sample for the ImageNet-200. When training with synthetic negatives we follow the two step procedure as explained in Section 4 of the main manuscript. We use the DenseFlow-25-6 [47] to generate synthetic samples. We pretrain the flow on inlier images, e.g. CIFAR-10 or ImageNet-200, for 300 epoch following the hyperparameters from [47]. In the first step, we jointly train the flow pretrained on inlier images and a randomly initialized K-way classifier with the ResNet-18 backbone according to Equation 6 from the main manuscript. We train for 100 epochs and use the same hyperparameters as described above. In the second step, we freeze the flow and add the K+1-th logit to the classifier and finetune for 20 epochs. We set the learning rate for the backbone to 0.0001 and 0.01 for the final fully connected layer. We set the loss modulation parameter from Equation 6 to 0.03.

E Additional results

We provide a discussion on the choice of negative data, an alternative implementation of negative objectness and the full results on the OpenOOD [102] benchmark.

E.1 Impact of synthetic negatives

Table 6 shows the performance of UNO depending on the source of negative training data. We experiment with random crops from inlier scenes, synthetic negatives generated by a jointly trained normalizing flow, and random instances from the ADE datasets. Training on synthetic negatives is more beneficial than training on inlier even though the flow was jointly trained only for a small number of iterations. For instance, training on inlier crops yields a high FPR₉₅ on Fishyscapes Lost&Found. Contrary, synthetic negatives yield low FPR₉₅ on all three validation sets. Still, there is a performance gap between models that are trained with and without real negative data.

Table 6: Performance of UNO for different training negatives in per-pixel outlier segmentation.

Training negatives	FS L&F		FS Static		RoadAnomaly	
	AP	FPR ₉₅	AP	FPR ₉₅	AP	FPR ₉₅
Inlier crops	67.2	62.5	79.2	0.9	86.5	7.6
Synthetic negatives	74.5	6.9	96.9	0.1	82.4	9.2
ADE20k negatives	81.8	1.3	98.0	0.04	88.5	7.4

E.2 Alternative implementation of the outlier posterior

The outlier posterior $P(y_{\text{NO}}|\mathbf{z})$ can alternatively be modeled with an additional out-of-distribution head [4]. Then, we introduce an additional binary cross-entropy loss term to train the out-of-distribution head that discriminates inliers and outliers. This way the closed set classifier ends up with K classes and is not affected by the negative data. When applied to the mask-wide recognition architecture, the OOD head has 3 outputs 1) inlier, 2) outlier and 3) no-object. Table 7 shows the comparison of the K+2-way classifier proposed in the main paper with a K+1-way classifier and a 3-way OOD head and ablation of UNO components in the pixel-wise outlier detection setup. Our original UNO formulation built atop K+2-way classifier consistently outperforms alternative formulations across all datasets and metrics.

Table 7: Comparison of the K+2-way classifier with the OOD head atop of Mask2Former architecture on Fishyscapes val and RoadAnomaly.

Method	Score	FS L&F		FS Static		RoadAnomaly	
		AP	FPR ₉₅	AP	FPR ₉₅	AP	FPR ₉₅
K+2-way classifier	s_{UNO}	81.8	1.3	98.0	0.0	88.5	7.4
K-way classifier & OOD head	s_{UNO}	81.4	5.3	89.0	0.3	80.6	10.6
K-way classifier & OOD head	s_{Unc}	77.8	2.2	86.4	1.6	76.1	8.4
K-way classifier & OOD head	s_{NO}	79.9	7.3	88.3	0.3	74.5	25.2

Table 8 presents a similar analysis in the image-wide setting using the OpenOOD CIFAR-10 setup. Again, the K+1-way classifier combined with our UNO score outperforms the K-way classifier and a binary OOD head. Still, our UNO score works well even with the alternative formulation.

Table 8: Comparison of the K+1-way classifier with the binary OOD head atop of ResNet-18 on OpenOOD CIFAR-10. We use UNO as the outlier score.

Method	Near-OOD		Far-OOD	
	AUC	FPR ₉₅	AUC	FPR ₉₅
K+1-way classifier	95.00	18.75	97.95	9.30
K-way classifier & OOD head	94.23	19.31	97.76	11.12

E.3 Full results on OpenOOD

Tables 9 and 10 provide the extended results on the OpenOOD [102] benchmark. We compare with post-hoc methods (upper section) and training methods without (middle section) and with the use of real negative data (bottom section). All results are averaged over three runs with variances in subscripts.

Table 9: OOD detection performance on the OpenOOD benchmark, the CIFAR-10 dataset.

Method	Near-OOD			Far-OOD			Acc.
	AUC	FPR ₉₅	AP	AUC	FPR ₉₅	AP	
OpenMax [0]	87.62(±0.29)	43.62(±2.27)	80.60(±0.29)	89.62(±0.19)	29.69(±1.21)	90.19(±0.41)	95.06(±0.30)
MSP [63]	88.03(±0.25)	48.17(±3.92)	85.43(±0.36)	90.73(±0.43)	31.72(±1.84)	93.27(±0.14)	95.06(±0.30)
TempScale [65]	88.09(±0.31)	50.96(±4.32)	86.11(±0.33)	90.97(±0.52)	33.48(±2.39)	93.68(±0.11)	95.06(±0.30)
ODIN [60]	82.87(±1.85)	76.19(±6.08)	83.03(±1.15)	87.96(±0.61)	57.62(±4.24)	93.14(±0.44)	95.06(±0.30)
MDS [68]	84.20(±2.40)	49.90(±3.98)	79.88(±3.18)	89.72(±1.36)	32.22(±3.40)	93.81(±0.74)	95.06(±0.30)
MDSEns [62]	60.43(±0.26)	92.26(±0.20)	59.94(±0.19)	73.90(±0.27)	61.47(±0.48)	83.37(±0.04)	95.06(±0.30)
RMDS [49]	89.80(±0.28)	38.89(±2.39)	87.52(±0.29)	92.20(±0.21)	25.35(±0.73)	94.21(±0.10)	95.06(±0.30)
Gram [61]	58.66(±4.83)	90.87(±1.91)	57.57(±5.09)	71.73(±3.20)	72.34(±6.73)	82.89(±3.14)	95.06(±0.30)
EBO [64]	87.58(±0.46)	61.34(±4.63)	87.04(±0.27)	91.21(±0.92)	41.69(±5.32)	94.31(±0.09)	95.06(±0.30)
OpenGAN [60]	53.71(±7.68)	94.48(±4.01)	53.35(±5.22)	54.61(±15.51)	83.52(±11.63)	73.34(±8.49)	95.06(±0.30)
GradNorm [47]	54.90(±0.98)	94.72(±0.82)	57.95(±1.98)	57.55(±3.22)	91.90(±2.23)	76.75(±1.95)	95.06(±0.30)
ReAct [89]	87.11(±0.61)	63.56(±7.33)	86.65(±0.19)	90.42(±1.41)	44.90(±8.37)	93.99(±0.45)	95.06(±0.30)
MLS [62]	87.52(±0.47)	61.32(±4.62)	86.88(±0.29)	91.10(±0.89)	41.68(±5.27)	94.21(±0.06)	95.06(±0.30)
KLM [62]	79.19(±0.80)	87.86(±6.37)	80.37(±0.46)	82.68(±0.21)	78.31(±4.84)	90.57(±0.25)	95.06(±0.30)
VIM [92]	88.68(±0.28)	44.84(±2.31)	86.32(±0.39)	93.48(±0.24)	25.05(±0.52)	96.27(±0.24)	95.06(±0.30)
KNN [62]	90.64(±0.20)	34.01(±0.38)	88.50(±0.35)	92.96(±0.14)	24.27(±0.40)	94.93(±0.07)	95.06(±0.30)
DICE [62]	78.34(±0.79)	70.04(±7.64)	74.80(±2.33)	84.23(±1.89)	51.76(±4.42)	89.06(±1.72)	95.06(±0.30)
RankFeat [64]	79.46(±2.52)	60.88(±4.60)	74.46(±3.08)	75.87(±5.06)	57.44(±7.99)	81.27(±3.67)	95.06(±0.30)
ASH [62]	75.27(±1.04)	86.78(±1.82)	77.24(±1.26)	78.49(±2.58)	79.03(±4.22)	88.33(±1.39)	95.06(±0.30)
SHE [102]	81.54(±0.51)	79.65(±3.47)	82.04(±0.51)	85.32(±1.43)	66.48(±5.98)	91.26(±0.04)	95.06(±0.30)
ConfBranch [45]	89.84(±0.24)	31.28(±0.66)	85.50(±0.30)	92.85(±0.29)	94.88(±0.05)	93.48(±0.39)	94.88(±0.05)
RotPred [101]	92.68(±0.27)	28.14(±1.68)	90.47(±0.35)	96.62(±0.18)	12.23(±0.33)	97.54(±0.13)	95.35(±0.52)
G-ODIN [45]	89.12(±0.57)	45.54(±2.52)	88.25(±0.49)	95.51(±0.31)	21.45(±1.91)	97.35(±0.34)	94.70(±0.25)
CSI [86]	89.51(±0.19)	33.66(±0.64)	86.37(±0.25)	92.00(±0.30)	26.42(±0.29)	93.90(±0.33)	91.16(±0.14)
ARPL [101]	87.44(±0.15)	40.33(±0.70)	82.96(±0.33)	89.31(±0.32)	32.39(±0.74)	91.41(±0.09)	93.66(±0.11)
MOS [64]	71.45(±3.09)	78.72(±5.86)	72.41(±3.05)	76.41(±5.93)	62.90(±6.62)	85.24(±2.92)	94.83(±0.37)
VOS [62]	87.70(±0.48)	57.03(±1.92)	86.57(±0.73)	90.83(±0.92)	40.43(±4.53)	93.95(±0.56)	94.31(±0.64)
LogitNorm [92]	92.33(±0.08)	29.34(±0.81)	90.62(±0.09)	96.74(±0.06)	13.81(±0.20)	97.29(±0.21)	94.30(±0.25)
CIDER [101]	90.71(±0.16)	32.11(±0.94)	87.97(±0.24)	94.71(±0.36)	20.72(±0.85)	96.19(±0.19)	-
NPOS [89]	89.78(±0.33)	32.64(±0.70)	86.36(±0.68)	94.07(±0.49)	20.59(±0.69)	96.20(±0.43)	-
UNO (ours)	91.34(±0.33)	31.78(±0.82)	87.39(±0.35)	92.55(±0.25)	20.54(±0.87)	93.96(±0.25)	95.20(±0.25)
MixOE [100]	88.73(±0.82)	51.45(±7.78)	94.25(±0.17)	91.93(±0.69)	33.84(±4.77)	98.00(±0.02)	94.55(±0.32)
MCD [97]	91.03(±0.12)	30.17(±0.06)	87.73(±0.36)	91.00(±1.10)	32.03(±4.21)	94.45(±0.85)	94.95(±0.04)
UDG [62]	89.91(±0.25)	35.34(±0.95)	86.89(±0.84)	94.06(±0.90)	20.35(±2.41)	95.23(±0.89)	92.36(±0.84)
OE [62]	94.82(±0.21)	19.84(±0.95)	87.39(±0.60)	96.00(±0.13)	13.13(±0.53)	95.03(±0.12)	94.63(±0.26)
UNO (ours)	94.87(±0.07)	9.33(±0.50)	94.49(±0.13)	97.63(±0.72)	9.38(±2.65)	99.10(±0.25)	94.88(±0.19)

Table 10: OOD detection performance on the OpenOOD benchmark, the Imagenet-200 dataset.

Method	Near-OOD			Far-OOD			Acc.
	AUC	FPR ₉₅	AP	AUC	FPR ₉₅	AP	
OpenMax [4]	80.27(±0.10)	63.48(±0.25)	81.42(±0.19)	90.20(±0.17)	33.12(±0.66)	85.13(±0.47)	86.37(±0.08)
MSP [68]	83.34(±0.06)	54.82(±0.35)	85.95(±0.05)	90.13(±0.09)	35.43(±0.38)	88.71(±0.14)	86.37(±0.08)
TempScale [65]	83.69(±0.04)	54.82(±0.23)	86.29(±0.02)	90.82(±0.09)	34.00(±0.37)	89.49(±0.15)	86.37(±0.08)
ODIN [60]	80.27(±0.08)	66.76(±0.26)	85.02(±0.03)	91.71(±0.19)	34.23(±1.05)	91.29(±0.15)	86.37(±0.08)
MDS [68]	61.93(±0.51)	79.11(±0.31)	67.68(±0.42)	74.72(±0.26)	61.66(±0.27)	70.80(±0.61)	86.37(±0.08)
MDSEns [68]	54.32(±0.24)	91.75(±0.10)	64.81(±0.24)	69.27(±0.57)	80.96(±0.38)	69.62(±0.52)	86.37(±0.08)
RMDS [74]	82.57(±0.25)	54.02(±0.58)	83.07(±0.45)	88.06(±0.34)	32.45(±0.79)	82.71(±0.78)	86.37(±0.08)
Gram [84]	67.67(±1.07)	86.40(±1.21)	75.63(±0.78)	71.19(±0.24)	84.36(±0.78)	72.75(±0.25)	86.37(±0.08)
EBO [65]	82.50(±0.05)	60.24(±0.57)	85.48(±0.07)	90.86(±0.21)	34.86(±1.30)	89.85(±0.21)	86.37(±0.08)
OpenGAN [60]	59.79(±3.39)	84.15(±3.85)	66.85(±2.79)	73.15(±4.07)	64.16(±9.33)	66.62(±3.69)	86.37(±0.08)
GradNorm [64]	72.75(±0.82)	82.67(±0.30)	80.19(±0.68)	84.26(±0.87)	66.45(±0.22)	86.54(±0.92)	86.37(±0.08)
ReAct [82]	81.87(±0.98)	62.49(±2.19)	85.38(±0.34)	92.31(±0.56)	28.50(±0.95)	91.31(±0.80)	86.37(±0.08)
MLS [65]	82.90(±0.04)	59.76(±0.59)	85.96(±0.07)	91.11(±0.19)	34.03(±1.21)	90.10(±0.21)	86.37(±0.08)
KLM [64]	80.76(±0.08)	70.26(±0.64)	83.41(±0.23)	88.53(±0.11)	40.90(±1.08)	84.22(±0.47)	86.37(±0.08)
VIM [75]	78.68(±0.24)	59.19(±0.71)	81.61(±0.29)	91.26(±0.19)	27.20(±0.30)	90.01(±0.35)	86.37(±0.08)
KNN [65]	81.57(±0.17)	60.18(±0.52)	85.72(±0.17)	93.16(±0.22)	27.27(±0.75)	93.48(±0.15)	86.37(±0.08)
DICE [63]	81.78(±0.14)	61.88(±0.67)	85.37(±0.13)	90.80(±0.31)	36.51(±1.18)	90.55(±0.29)	86.37(±0.08)
RankFeat [82]	56.92(±1.59)	92.06(±0.23)	66.17(±1.63)	38.22(±3.85)	97.72(±0.75)	45.25(±2.81)	86.37(±0.08)
ASH [72]	82.38(±0.19)	64.89(±0.90)	87.03(±0.06)	93.90(±0.27)	27.29(±1.12)	94.15(±0.32)	86.37(±0.08)
SHE [102]	80.18(±0.25)	66.80(±0.74)	84.20(±0.28)	89.81(±0.61)	42.17(±1.24)	90.05(±0.62)	86.37(±0.08)
ConfBranch [14]	79.10(±0.24)	61.44(±0.34)	82.11(±0.30)	90.43(±0.18)	34.75(±0.63)	88.67(±0.27)	85.92(±0.07)
RotPred [14]	81.59(±0.20)	60.42(±0.60)	84.87(±0.19)	92.56(±0.09)	26.16(±0.38)	90.10(±0.08)	86.37(±0.16)
G-ODIN [15]	77.28(±0.10)	69.87(±0.46)	82.77(±0.16)	92.33(±0.11)	30.18(±0.49)	92.04(±0.10)	84.56(±0.28)
ARPL [14]	82.02(±0.10)	55.74(±0.70)	84.35(±0.08)	89.23(±0.11)	36.46(±0.08)	87.63(±0.19)	83.95(±0.32)
MOS [16]	69.84(±0.46)	71.60(±0.48)	73.38(±0.56)	80.46(±0.92)	51.56(±0.42)	72.79(±1.43)	85.60(±0.20)
VOS [75]	82.51(±0.11)	59.89(±0.47)	85.59(±0.07)	91.00(±0.28)	34.01(±0.97)	90.11(±0.30)	86.23(±0.19)
LogitNorm [92]	82.66(±0.15)	56.46(±0.37)	86.41(±0.08)	93.04(±0.21)	26.11(±0.52)	92.25(±0.32)	86.04(±0.15)
CIDER [14]	80.58(±1.75)	60.10(±0.73)	83.32(±1.76)	90.66(±1.68)	30.17(±2.75)	89.16(±2.38)	-
NPOS [88]	79.40(±0.39)	62.09(±0.05)	84.37(±0.35)	94.49(±0.07)	21.76(±0.21)	94.83(±0.07)	-
UNO (ours)	81.16(±0.65)	61.10(±0.93)	85.31(±0.94)	92.53(±0.48)	32.32(±0.19)	87.24(±0.33)	86.33(±0.36)
OE [68]	84.84(±0.16)	52.30(±0.67)	86.86(±0.22)	89.02(±0.18)	34.17(±0.56)	85.15(±0.26)	85.82(±0.21)
MCD [77]	83.62(±0.09)	54.71(±0.83)	84.44(±0.30)	88.94(±0.10)	29.93(±0.30)	82.90(±0.48)	86.12(±0.17)
UDG [95]	74.30(±1.63)	68.89(±1.72)	78.09(±2.02)	82.09(±2.78)	62.04(±5.99)	81.63(±3.29)	68.11(±1.24)
MixOE [101]	82.62(±0.03)	57.97(±0.40)	84.78(±0.05)	88.27(±0.41)	40.93(±0.29)	86.01(±0.60)	85.71(±0.07)
UNO (ours)	85.07(±0.78)	51.71(±0.31)	85.29(±0.71)	89.63(±0.46)	36.79(±0.21)	87.07(±0.14)	86.42(±0.32)